SI-referenced formic acid (HCOOH) spectroscopy at the sub ppt level

Maxime Leuliet, Abdessamad Mbardi, Bérengère Argence, Jean-Philippe Karr, Laurent Hilico

SI-referenced HCOOH spectroscopy at the sub ppt level.

Maxime Leuliet[1], Abdessamad Mbardi[1], Bérengère Argence[1], Jean-Philippe Karr[1,2], and Laurent Hilico[1,2]

[1]Laboratoire Kastler Brossel, Sorbonne Université, CNRS, ENS-PSL Research University, Collège de France, 4 place Jussieu, F-75005 Paris, France
[2]Université d'Evry-Val d'Essonne, Université Paris-Saclay, Boulevard François Mitterrand, F-91000 Evry, France

September 13, 2024

Abstract

We report on a new determination of the ν_6, $J' = 21, K'_a = 2, K'_c = 20 \leftarrow J'' = 21, K''_a = 3, K''_c = 19$ HCOOH rovibrational line at 9.17 μm with 40-fold improvement with respect to previous measurements, using a Fabry-Prot saturated-absorption spectrometer referenced to the Système International through a frequency comb The relative resolution is better than 3. 10^{-13}. We elaborate a detailed line shape model that allows retrieving the expected transit time width and accurate determination of the pressure and power shifts and broadenings.

1 Introduction

Optical fiber telecommunication networks enable *Système International* (SI)-referenced ultra stable optical signals around 1.5 μm to be disseminated from national metrology institutes to remote laboratories with stabilities better than 10^{-15} for integration times larger than 1 s and long term accuracies better than 10^{-19} [1]. These features can be transferred to all the teeth of optical frequency combs and hence to any laser which is frequency controlled against the frequency comb, allowing for SI-referenced high resolution spectroscopy [2, 3].

The French REFIMEVE ultrastable signal has recently been delivered at Kastler Brossel laboratory on Jussieu campus in Paris and used for this work. In this paper, we present the optical frequency synthesis spectrometer we have built for molecular spectroscopy at 9.17 μm and the measurement campaign performed on the ν_6, $J' = 21, K'_a = 2, K'_c = 20 \leftarrow J'' = 21, K''_a = 3, K''_c = 19$ formic acid - HCOOH - rovibrational line.

The experimental setup is described in section 2. It presents the SI-referenced CO_2 laser system, the saturated absorption cell, the frequency modulation method and the resulting spectroscopy signal. In section 3, we discuss the lineshape model used to adjust the recorded spectra. The results are presented and discussed in section 4. We obtain a sub ppt (10^{-12}) frequency resolution on the line center. SECTION 5, SECTION 6

2 Experimental setup

2.1 SI-referenced laser system

The spectroscopy laser is a CO_2 laser frequency controlled against a frequency comb which is optically stabilized to the REFIMEVE ultrastable signal referenced to the système international (SI) [2]. The setup is described in Fig. 1. The 1542 nm ultrastable signal disseminated by the REFIMEVE network is phase noise compensated up to the extraction station located next to our laboratory with an expected relative frequency stability better that 10^{-15} for integration times larger than 1 s. We use a 102 m non-compensated single mode fiber to bring the ultrastable signal to our lab in the same building, which slightly reduces the REFIMEVE frequency stability that remains better than 10^{-14}. The frequency of the REFIMEVE ultrastable signal is ν_R=194 400 008 500 000±2 Hz under standard REFIMEVE operating conditions. We also receive a SI-referenced 100 MHz signal from Paris Observatory. REF This signal is used to phase lock a f_Q=10 MHz

quartz oscillator used to synchronize all the instruments. The relative stability of this quartz oscillator is better than 5×10^{-13} for integration times larger than 1 s.

The laser source is a single mode CO_2 laser operated on the 9R(42) line with up to 800 mW of optical power. The optical cavity is made of a 150 groves/mm grating in the Littrow configuration for line selection and of a rear mirror mounted on a piezo ceramic split in two zones, a short one for fast frequency control and a long one to compensate slow drifts. The CO_2 laser beam is then split into three parts. The first one allows its frequency control against a 1.5-1.9 μm frequency comb as described in figure 1. The second one is frequency shifted by +128 MHz using a double pass acousto-optic modulator (AOM) instead of a single pass AOM in [4] to probe the HCOOH molecular transition discussed in this paper. The third one is used to control the frequency of a quantum cascade laser to perform H_2^+ vibrational spectroscopy, not described in this work.

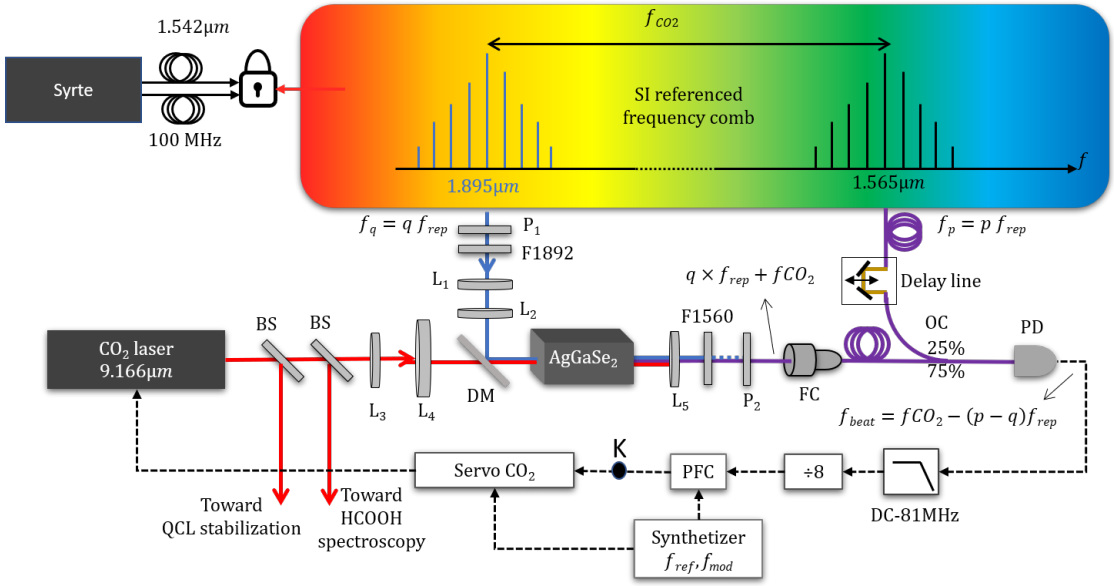

Figure 1: Experimental setup for the stabilization of the CO_2 laser onto the SI-referenced frequency comb. The 9.166 μm CO_2 beam is overlapped with the 1.895 μm part of the frequency comb for sum frequency mixing in a $AgGaSe_2$ crystal. The shifted comb at 1.565 μm is combined with the original comb at 1.565 μm to produce a beat note on the photodetector. This beat note is used to lock the CO_2 laser via a phase lock loop. L_i: Lenses, P_i: Polarizers, DM: dichroic mirror, BS: beam splitter, FC: fiber collimator, OC: optical coupler, PD: photodetector, PFC: phase/frequency comparator. K: phase/frequency error signal used in Fig. 3.

The optical frequency comb consists of an erbium-doped fibre mode-locked laser emitting around 1.56 µm (TOPTICA DFC CORE 200) with a repetition rate f_{rep}= 200 MHz. Thanks to the use of a difference frequency generation method, the comb is carrier enveloppe offset frequency-free. The comb teeth frequencies are thus given by pf_{rep} where p is the tooth order. The comb can be operated in RF-lock mode and the repetition frequency is referenced to the quartz frequency f_Q or in optical lock mode. In the latter case, the comb is phase-locked to the REFIMEVE ultrastable signal using a beat note between the REFIMEVE signal and the tooth of order p_0 of the comb. The beat note frequency is $f^R_{beat} = \nu_R - p_0 f_{rep}$. With p_0=974 000 and a f^R_{beat}=8.5 MHz, f_{rep} is exactly set to 200 MHz. The frequency stability of the comb, locked on the ultrastable REFIMEVE signal, is thus expected to be at the 10^{-14} level or even lower for integration times larger than 1 s.

In RF-lock mode, the feedback loop has a very small bandwith of less than 1 Hz in order to long term lock the repetition rate without degrading the free running stability of the comb [5]. The RF-locked comb to REFIMEVE beat note line shape exhibit a Voigt profile with a FWHM of 43,5 kHz (24.3 kHz lorentzian and 28.3 kHz gaussian contributions). In optical-lock mode, the comb teeth are tightly locked to the ultrastable signal with a 580 kHz bandwidth, thus transfering the ultrastable signal spectral charateristics to the comb. All the measurements are performed in optical-lock mode. The optical lock mode improves the spectrometer resolution by a factor 4.8 with respect to the RF lock mode as examplified in Fig. 6.

An ouput of the comb is injected in a comb extension (TOPTICA DFC EXT) where it is amplified and sent to a highly non linear fiber to generated an additional comb output at 1.9 µm. The CO_2 laser beam is superimposed and mode matched to the 1.9 μm part of the frequency

comb in a 8 mm long $AgGaSe_2$ crystal. With 87 mW of CO_2 laser radiation and 18.4 mW in 56 nm around 1895 nm we generate about 1.1 μW of sum frequency comb radiation at 1.56 nm, corresponding to a conversion efficiency of 0.7 mW/W^2. This radiation is spectrally filtered with a 54 nm wide bandpass filter and injected into an optical fiber. An optical delay line ensures the temporal matching between the pulses of the sum frequency comb and the original one. The combs are then mixed in a 75/25% fiber combiner and sent to a fast photodetector for beat note detection. The original and shifted comb frequencies have the form $\nu_p = pf_{rep}$ and $\nu_q = qf_{rep} + \nu_{CO_2}$. The beat signal contains peaks at $f_{beat}^{CO_2} = \nu_{CO_2} - (p-q)f_{rep}$. The lowest positive beat frequency is close to 64 MHz and is obtained for $p - q = 163\,541$. This comb to comb beat is shown in Fig 2. It has a signal to noise ratio up to 58 dB in a 30 kHz resolution bandwidth (or 53 dB in 100 kHz RBW). It is bandpass filtered, divided by 8 and compared to a reference frequency f_{ref} from a synthesizer using a phase/frequency comparator to obtain a phase error signal. The CO_2 laser servo loop includes a proportional-integral path to the short piezo part, with a loop oscillation frequency of 9 kHz. A second pure integrator slowly acts on the long piezo zone to maintain the fast piezo correction within its working range.

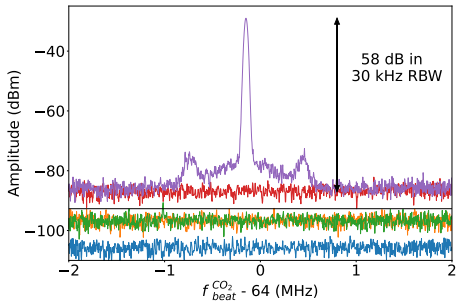

Figure 2: Beat note between the original and shifted combs around 64 MHz (purple). Blue: analyzer noise floor, green: electronic noise, orange: electronic + shifted comb noise, black line: expected shot noise, red: electronic + comb noise, purple: beatnote signal. Resolution bandwidth RBW = 30 kHz. The side peaks at 580 kHz from the carrier are remnants of the comb to REFIMEVE optical lock.

2.2 Saturated absorption setup

The HCOOH saturated absorption setup is shown in Fig. 3. It is performed in a 1.047 m long symmetric Fabry-Perot cavity installed in a vacuum vessel. The mirrors have a 50 m radius of curvature resulting in a beam waist $w_0 = 3.85$ mm. The CO_2 laser is injected into the Fabry-Perot cavity with a linear horizontal polarization and mode-matched using a telescope. The beam transmitted by the cavity is detected using a liquid nitrogen cooled HgCdZnTe detector and a transimpedance amplifier. The transmitted signal expressed in volts gives a precise relative scale for the intracavity power or intensity but only an approximate absolute scale of 1.44(14) mW/V for the total power P_o and 0.0618(62) mW/mm^2/V for the intensity on the beam axis I given by $I = 2P_o/(\pi w_0^2)$. The data analysis is made using the precise scale and the results are converted in physical units with larger uncertainties.

To get stable HCOOH pressure during the measurements, we use a leak valve to inject HCOOH from a small reservoir containing liquid HCOOH and a turbo pump connected to the vacuum vessel through a valve. Both valves are adjusted to get a stable pressure to better than 1% in the vacuum vessel. We have determined the HCOOH single pass absorption by measuring the cavity maximum transmission for different HCOOH pressures and found 7.43×10^{-3} μb^{-1} corresponding to an absorption of 7.1×10^{-3} m$^{-1}\mu$b^{-1}. The empty cavity finesse is 153. The cavity finesse varies from 143 to 119 when we vary the HCOOH pressure from 0.5 to 2 μb. Note that HCOOH can be considered to be a pure gas at room temperature with a dimer fraction below 0.13% at 2μb [6], see Sect. 8.

To perform spectroscopy, the Fabry-Perot cavity is locked on resonance with the CO_2 laser frequency using first harmonic phase sensitive detection at 33 kHz of the signal transmitted by the cavity. The HCOOH saturated absorption signal is detected using a third harmonic phase sensitive detection (Stanford research SR810). To that end, the reference frequency f_{ref} given by the synthesizer is frequency modulated with a modulation frequency f_m and a modulation depth δf_m. Since the modulation is transferred to the CO_2 laser frequency by the feedback loop, the

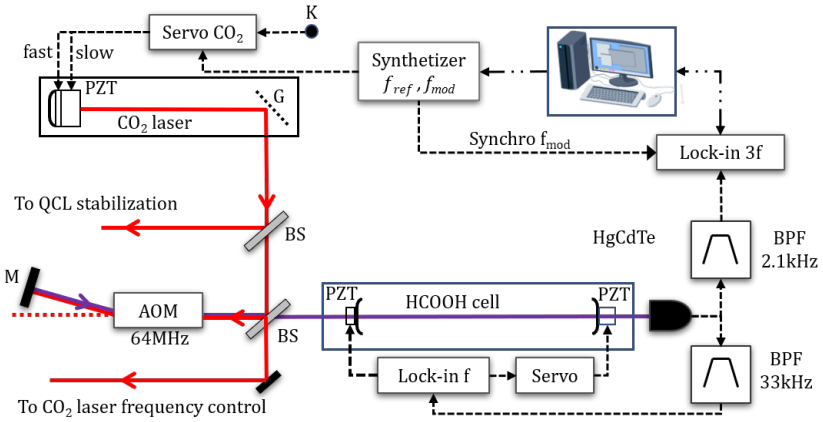

Figure 3: HCOOH spectrometer. BS: beam splitter, G: grating, BPF: band pass filter, PZT: piezo transducer, K: error signal from Fig 1. Full lines: laser beams, dashed lines: electronic signals, double dotted line: data transfer.

actual modulation depth is precisely determined well within 20 Hz analysing the FM sideband heights appearing in the comb to comb beatnote.

2.3 Experimental spectra

We have systematically recorded spectra for four different HCOOH pressures, four different laser intensities, three different modulation frequencies (110, 220 and 330 Hz) and three different modulation depths (20, 40 and 60 kHz) with five scans up and five scans down totaling 1440 scans, 4 of which are shown in Fig. 4. Each scan is made of 178 steps with 160 small 2.5 kHz frequency steps near the center of the line and 9 larger steps to probe the wings on both sides and detect an offset if any. The third harmonic phase sensitive detection time constant is set to 30 ms with a -24 dB/octave roll-off and the dwell time between two measurements is set to 340 ms, larger than the PSD settling time of 300 ms. The noise equivalent bandwidth is 2.6 Hz (from SR810 user's manual). For each line, we evaluate the signal to noise ratio (in the 2.6 Hz equivalent bandwidth) as the ratio of the maximum of the signal to the rms of the signal in the wings. It varies from 20 for high pressure, high laser power and low modulation depth up to 363 at low pressure, low intensity and large modulation depth. Right before and right after each scan, the HCOOH pressure and transmitted power are measured. These values are used whenever necessary in the spectrum adjustment procedure.

3 Lineshape model

The formic acid line studied here is ν_6 vibrational band, (J' = 21, Ka' = 2, Kc' = 20) $\leftarrow$ (J" = 21, Ka" = 3, Kc" = 19). This line is a well isolated line within the $\approx$ 40 MHz Doppler width of HCOOH at room temperature, so no line pulling is expected. The spectroscopy we perform is in the so called wavelength modulation regime with modulation and demodulation frequencies of at most 310 and 930 Hz, much smaller than the lower limit of the linewidth fixed by the transit time of the molecules in the laser beam profile characterized by a Lorentzian profile with a half width at half maximum (HWHM) given by [7]

$$\Delta\nu_{tr}^{th} = \frac{\sqrt{2ln(2)}}{2\pi w_0}\sqrt{\frac{2k_BT}{m}} = 15.8(10)\ \text{kHz}, \tag{1}$$

if probed by a non modulated laser at $T = 300$ K. The actual transition width $\Delta\nu$ is larger than the limit given by Eq. (1) due to additional pressure, power and modulation broadening.

The third derivative of a Lorentzian profile we can expect is perturbed by three effects. The first one is line shape distortion due to frequency modulation described by Arndt [8] (see section 6.1 for details) leading to the line shape

$$S_n(x,m) = \frac{i^n\epsilon_n}{2\ m^n}\frac{(\sqrt{(1-ix)^2+m^2}-(1-ix))^n}{\sqrt{(1-ix)^2+m^2}} + c.c., \tag{2}$$

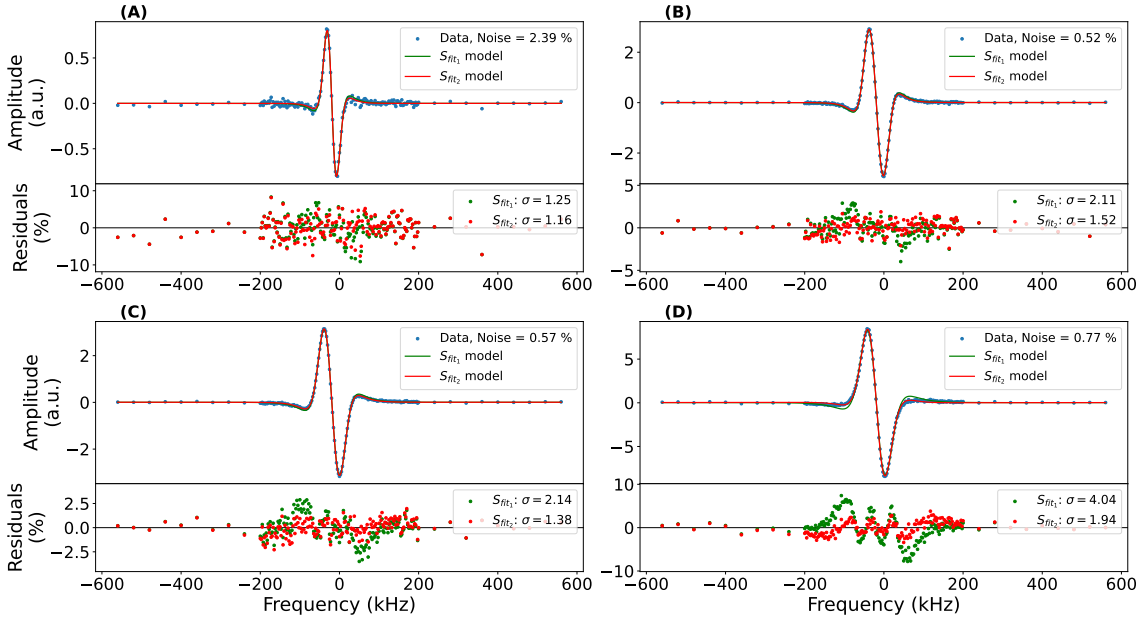

Figure 4: Examples of saturated absorption spectra detected in third harmonic. Experimental parameters (modulation frequency, modulation depth, pressure, power) are A: (XXX, 20 kHz, 0.5 μb, 0.5 V), B: (XXX, 40 kHz, 0.5 μb, 0.5 V), C: (XXX, ?? kHz, 1.0 μb, 0.5 V) and D: (XXX, ?? kHz, 1.0 μb, 2.0 V). The noise level, estimated from the standard deviation in the wings of the spectra, is given as a percentage of the maximum signal. The profiles are fitted by the S_{fit} model (red solid line). The residuals are represented as a percentage of the maximum signal. Horizontal axis: $\nu - \nu_{off}$ with ν_{off} = 32 708 391 980 825 Hz.

where $x = (\nu - \nu_c)/\Delta\nu$ is the normalized laser detuning with respect to the transition frequency ν_c, $m = \delta\nu_m/\Delta\nu$ is the normalized modulation depth and n is the phase sensitive detection order with $\epsilon_0 = 1$ and $\epsilon_{n\geq 1} = 2$. The second effect is combined intensity-frequency modulation (IM-FM) due to the Fabry-Perot cavity. Since the Fabry-Perot cavity is locked on resonance with the laser frequency, the transmitted intensity varies quadratically with frequency around the transmission maximum, and thus the laser frequency modulation at frequency f_m is turned into an intensity modulation at frequency $2f_m$. As a result, contributions of S_1 and S_5 type are added to the S_3 line shape in the case of third harmonic detection. The third effect, which cannot be included in the lineshape model is line distortion due to unresolved hyperfine structure. It is discussed in section 4.3.

The expected line shape including the modulation distortion and IM-FM effects is derived in section 6.2, Eq. (30) and reads:

$$S_{fit}(A_0, A, \nu_c, \Delta\nu) = A_0 - A\left(\frac{qm^2}{4}S_1(x,m) + (1+\frac{qm^2}{2})S_3(x,m) + \frac{qm^2}{4}S_5(x,m)\right) \quad (3)$$

It depends on four adjustable parameters, a possible vertical offset A_0 of the signal, a global amplitude A, the central frequency ν_c that appears in the normalized frequency x and the line HWHM $\Delta\nu$ that appears in the normalized frequency and in the normalized modulation parameter m. The parameter $q = -4(\Delta\nu/\Delta\nu_{FP})^2$ defined in Eq. (15) depends on the Fabry-Perot HWHM $\Delta\nu_{FP}$ and hence on the formic acid pressure (see section 6.3.1 and Eq. (35)).

In the case of quantum cascade laser (QCL) spectroscopy, the observed lineshapes are asymetric due to phase/amplitude coupling and S_2 and S_4 terms would appear in the fitting function [9]. In our case, no line asymetry is allowed with S_{fit} functions. Indeed, thanks to the 128 MHz frequency shift introduced by the AOM (see Fig. 3), the CO_2 laser is swept around the intensity maximum of the CO_2 laser with zero phase/amplitude coupling. We have checked using first harmonic lockin detection that we have almost no detectable intensity modulation at the modulation frequency (intensity modulation to mean intensity below 10^{-5} at the output of the laser nor at the output of the Fabry-Perot cavity.

4 Results and discussion

The fits of the four chosen spectra with the S_{fit} profile together with their residuals are shown in Fig. 4. For each scan (labelled by $^{(j)}$), individual fit parameters $A_0^{(j)}$, $A^{(j)}$, $\nu_c^{(j)}$ and $\Delta\nu^{(j)}$ and error bars are obtained. The offsets A_0 are always negligible and we do not observe any systematic difference when comparing frequency scan up and frequency scan down. This absence of drag effect is due to the choice of a sufficiently long dwell time. The central frequencies ν_c and the line HWHM $\Delta\nu$ are displayed in Fig. 5 and 7. The different colors corresponds to the different modulation frequencies. The horizontal axis are split in three main columns (one for each modulation depth), which are in turn split in four columns (one for each HCOOH pressure), and finally split into four columns for each laser power. At this latter stage, in Fig. 5, the horizontal axis is used to display the individual values of ν_c whereas in Fig. 7 the horizontal scale locally represents the laser power and the points correspond to the HWHM averaged over the tens scans. The interest of this representation is to show the pressure and modulation depth trends.

In order to assess the symmetry of the line, for each spectra we have computed the correlation coefficient of the experimental data $S_{exp}(\nu - \nu_c)$ and the symmetrized data $S_{exp}(\nu_c - \nu)$ which is 1 for even functions and -1 for odd functions of $\nu - \nu_c$. We obtain correlation coefficients between ZZZ and ZZZZ indicating the high degree of symmetry of the line.

Figure 6 compares the central frequency histograms obtained operating the comb in the RF lock and optical lock modes for a given set of modulation, pressure an intensity parameters and exhibits a 4.9 fold improvement of the spectrometer resolution.

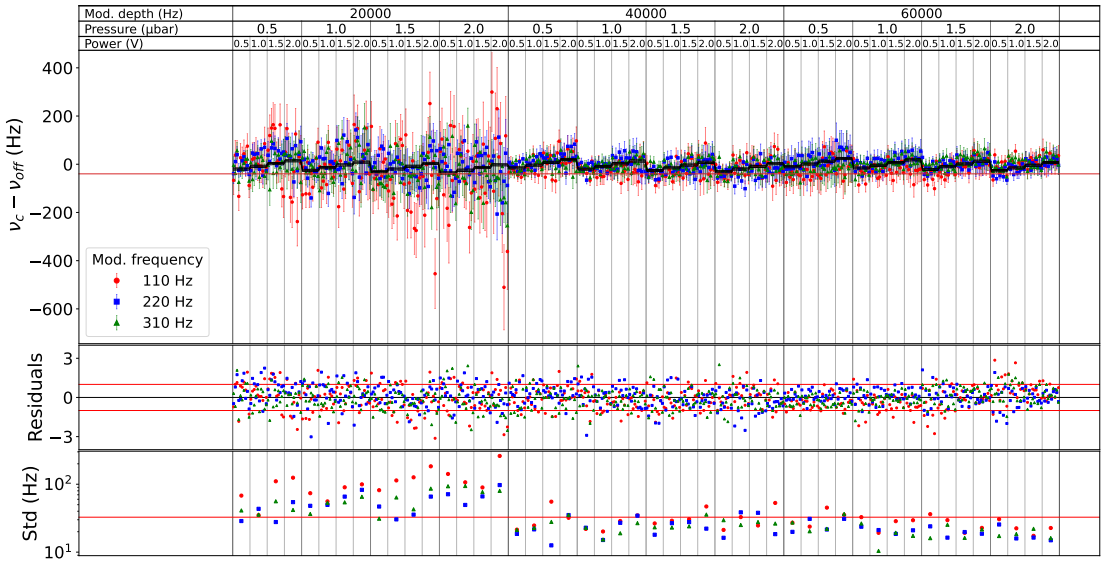

Figure 5: Top frame: central frequencies ν_c - ν_{off} and error bars obtained from saturated absorption spectra fitted by (top) the S_{fit} model given by Eq. (3) and (bottom) the S_{fit_2} model given by Eq. (3). They are plotted as a function of modulation depth, formic acid pressure in the Fabry-Perot cavity and intracavity laser power. Modulation frequency: 110 Hz (red points), 220 Hz (blue points), 310 Hz (green points).The thick black curve represents the multilinear fit of ν_c by Eq. (4) and the horizontal red solid line shows the estimated undisturbed central frequency ν_0 - ν_{off} with ν_{off} = 32 708 391 980 825 Hz. Middle frame: residuals of the multilinear fit, expressed in error bar unit. The red horizontal lines correspond to ±1 error bar. Bottom frame: standard deviation of the central frequency over the 10 scans performed for each quadruplet of parameter values. The horizontal red dashed line represents the 10^{-12} level, relatively to the transition frequency.

4.1 Central frequency analysis

The central frequencies and error bars obtained using the S_{fit} line profile for each of the 1440 scans performed with the different modulation frequencies, modulation depths, formic acid pressures P, intracavity intensities I and realisations are adjusted by a multilinear fit of the form

$$\nu_c^{(j)} = \nu_0 + af_{mod}^{(j)} + b\delta\nu_m^{(j)} + cP^{(j)} + dI^{(j)}. \quad (4)$$

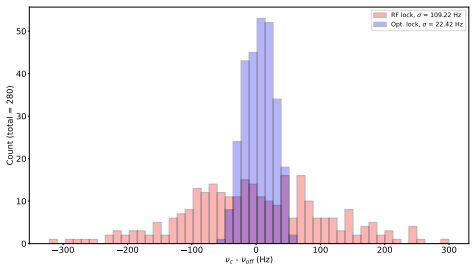

Figure 6: Histograms of central frequencies ν_c for RF-lock (pink) and optical lock (blue) comb regimes. Pressure xx μb, Intensity yyy V (zzz mW/mm^2), modulation frequency: ??, modulation depth: ??.

The fit is plotted in black in Fig. 5. For most points, the residuals are less than the error bars indicating an excellent agreement between the measured central frequencies and the multilinear adjustment.

The a, b, c and d parameters are given in Tab. 1. The modulation frequency shift coefficient a is very small and gives a shift of at most 12 Hz for $f_m = 310$ Hz. The modulation depth shift coefficient b is also very small and gives a shift of at most 15 Hz at 60 kHz modulation depth.

We obtain a very small pressure shift coefficient of ?? Hz/μb = ?? kHz/mT and a small light shift coefficient of ?? Hz/(mW/mm^2) which point out the excellent metrological features of the line (*THE PAPER CH3OH S. Y. Tochitsky and R. J. Butcher, "Precise measurements of line broadening and line shifts in low-pressure gases using a heterodyne CO2 laser spectrometer : Applications to C2H4 and CH3OH," Journal of the Optical Society of America B 15, 1392 (1998)* GIVES -0.52 kHz/mT for a CH3OH line next to 10P(16) of CO_2 laser).

The undisturbed central frequency ν_0 is given in Table 2. It has a statistical uncertainty of ?? Hz, i.e. ??$\times 10^{-13}$ in relative value. This represents at least a 100 fold improvement with respect to our previous measurement [10, 11]. The systematic uncertainty and comparison with our previous measurement and HITRAN database is discussed in Section LATER.

The last two columns of Table 1 and the last column of Table 2 show that the χ^2 of the fitted parameters (TO BE DEFINED) are closer to 1 for S_{fit_2} than for S_{fit_1} indicating that the former better fits the experimental data.

a	XXX	Hz/Hz
b	XXX	Hz/kHz
c	XXX	Hz/μb
d	XXX	Hz/V
d	XXX	Hz/(mW/mm^2)

Table 1: Multilinear fit parameters a, b, c and d obtained for the two fit functions defined in Eq. (3). d is either expressed in Hz/V with a 14 to 17% uncertainty or in Hz/(mW/mm^2) with a slightly larger 17 to 20% uncertainties.

ν_0 (Hz)	χ^2
32 708 391 980 785.2(4.5)	ZZ

Table 2: Central frequency ν_0 and statistical uncertainty.

4.2 Linewidth analysis

Figure 7 shows the HWHM $\Delta\nu^{(j)}$ averaged over the 10 scans registered for each modulation frequency, modulation depth, pressure and intensity quadruplet. They vary from XXX to XXX kHz and the corresponding m parameters from ZZZ to ZZZ. It clearly shows that the HWHM depends both on the pressure and the intensity but do not depend on the modulation depth, indicating that the S_{fit} profile well deconvolutes the modulation effect. Taking into account the pressure

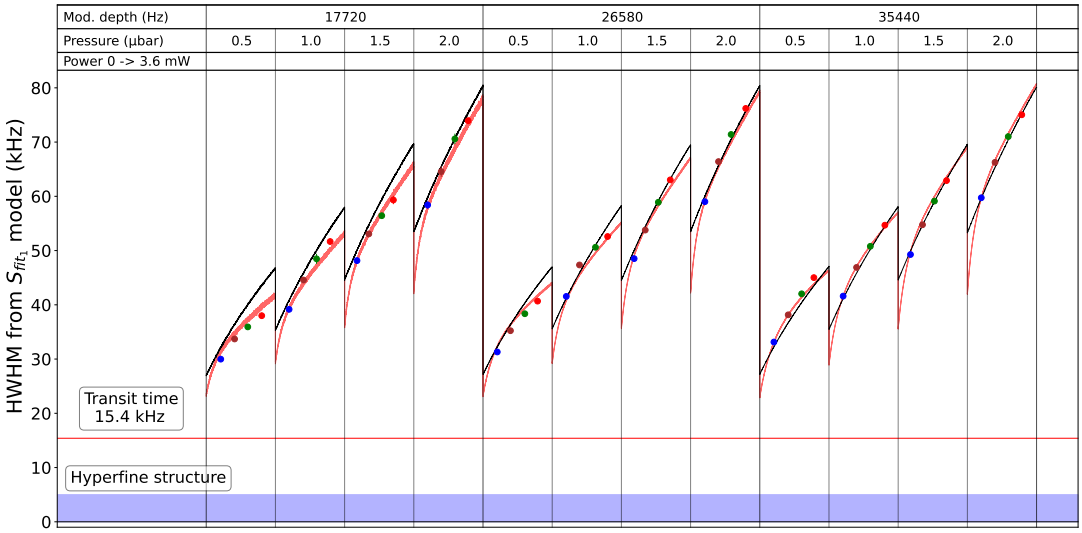

Figure 7: Averaged HWHM obtained by fitting the spectra with the S_{fit} profile. Dots with the same color share a comparable value of laser intensity. The black solid line is fit with ?? and the red solid line ??. The horizontal red line shows the estimated transit time HWHM of XX(X) kHz. The blue zone indicates the maximum expected hyperfine splitting, which is not resolved.

broadening and power broadening effects, the HWHM is expected to vary as [7]

$$\Delta\nu^{(j)} = (\Delta\nu_{tr} + \alpha P^{(j)})\sqrt{1 + \frac{I^{(j)}}{I_S}}, \tag{5}$$

with $\Delta\nu_{tr}$ the transit time HWHM, α the pressure broadening coefficient and I_S the saturation intensity of the line. A first determination of these parameters is obtained fitting the observed HWHM $\Delta\nu^{(j)}$ with Eq. (5). They are given in Table 3, column 2. The fit is plotted in black in Fig. 7. This HWHM analysis is not completely satisfactory for several reasons. First, the transit width we obtain, xx(X) kHz does not match the theoretical value 15.8(1.0) kHz. Secondly, the HWHM model of Eq. (5) does not well reproduce the observed HWHM power dependence, as shown by the black lines in Fig. 7. Finally, one can observe in Fig. 4 (B,C and D) that the S_{fit} model has non negligible residuals with reproducible wiggles indicating that the line shape model are not elaborated enough.

$\Delta\nu_{tr}$	XX(X)	XX(X)	kHz
α	XX(X)	XX(X)	kHz/μb
I_S	XX(X)	XX(X)	mW/mm^2
I'_S	—	XX(X)	mW/mm^2

Table 3: Preliminary (column 2) and final (column 3) determinations of the transit time HWHM $\Delta\nu_{tr}$, the pressure broadening coefficient α and the saturation intensities I_S and I'_S expressed in mW/mm^2.

4.3 Analysis including the hyperfine structure

Fitting trials have shown that introducing the sum of two S_{fit_2} profiles with different HWHM much improves the residuals in Fig. 4 and much better reproduce the HWHM power and pressure dependances with almost no impact on the central frequency determination. Even if unresolved, the hyperfine structure of the lines gives several contributions with close center frequencies and different widths that may explain the observations.

The hyperfine structure of HCOOH has been studied by Chardon [12] and Cazzoli [13] in the case of pure rotational spectroscopy in the ground vibrational level and led to the determination of

stat.			19 Hz
method			1 Hz
pressure	0.02 μbar	7.7 Hz/μb	0.2 Hz
power	30 mV	41.1 Hz/V	1.2 Hz
mod. depth	0.08 kHz	-6.4 Hz/kHz	< 5 Hz
polar.			
gas lens effect			20
			28 Hz

Table 4: Error budget on the deperturbed central frequency f_0. First column : origin of the contribution, second column: inaccuracy, third column: slope, fourth column: contribution to f_0 error.

coupling constants for rotational levels close to those probed in this work. In Section 7, we evaluate the hyperfine structure of the line studied here. It shows that the line shape can be modeled by the sum of three peaks of the form $S_{th}(x - x_i, m_i)$ given by Eq. (30) where $x - x_i = (\nu - \nu_i)/\Delta\nu_i$ and $m_i = \delta\nu_m/\Delta\nu_i$ with ν_1 = -4.4 kHz, ν_2 = 0.1 kHz and ν_3 = 4.6 kHz. Direct global fitting of the 1440 lines with this model involving fifteen parameters (a global offset, a central frequency, six amplitudes α_{ki} and the transit time width $\Delta\nu_{tr}$ with three pressure coefficients and three saturation intensities) is not possible due to the unresolved hyperfine structure and too high correlations between the numerous adjustable parameters.

Since the hyperfine splittings are much smaller than the transit HWHM, we model the lineshape as the sum of $N = 1$ to 4 S_{fit_1} functions with the same central frequency x_c^N but different amplitudes g_i^N and saturation intensities $I_{S,i}^N$ setting

$$S^N = \sum_i^N g_i^N S_{th}(x - x_c^N, m_i^N) + \alpha_0. \tag{6}$$

α_0 is a global offset and $m_i^N = \delta\nu_m/\Delta\nu_i^N$ where

$$\delta\nu_i^N = (\Delta\nu_{tr} + \alpha P)\sqrt{1 + \frac{I}{I_{S_i}^N}}. \tag{7}$$

S^N depends on ZZZ adjustable parameters, namely $\Delta\nu_{tr}$, α, β, $I_{S_1}^0$, $I_{S_2}^0$ as well as on the zero-pressure cavity HWHM $\Delta\nu_{FP}^0$ and its pressure coefficient η that have been determined experimentally (see section 6.3) to be $\Delta\nu_{FP}^0$ = 468 kHz and η = 67.5 kHz/μb.

4.3.1 Comment on $\Delta\nu_{tr}$ and α

4.3.2 Comment on saturation intensities

4.3.3 Checking the method

We have tried several other line profiles with sums of S_{fit} functions with different line centers, weights and widths. They all lead to the same determination of the line center within few Hz and to the same transit width?? and pressure broadening factor??.

4.4 Error budget

The error budget on the deperturbed central frequency f_0 is given in Table 4. The main contribution is the statistical uncertainty of 19 Hz obtained by fitting the central frequency f_c by Eq. (4). The contributions from pressure, intracavity intensity and modulation depth uncertainties are evaluated in the worst case

For the deperturbed central frequency : stat uncertainty, gas lens effect, For the central frequency under actual conditions: statsistics, gas lens effect, pressure, intensity and modulation contributions, other ideas ?

For the pressure broadening coefficient : ??

5 Conclusion

Using a SI-referenced frequency comb allowed to carry out a study of systematic effects of the pressure, the intensity and the modulation depth on the formic acid rovibrational transition central

ν_0 (kHz)	ref.
32 708 391 9xx.xxx(20)	this work
32 708 391 981.4(0.8)	[10]
32 708 394(3)	HITRAN [14]

Table 5: Central frequency ν_0 and statistical uncertainty.

Origin	Uncertainty	Uncertainty on $\Delta\nu$	
pressure	20 nbar	negligible	300 Hz
intracavity power	30 mV	1.2 Hz	< 460 Hz
modulation depth	2%	< 4.5 Hz	< 200 Hz

Table 6: Error budget on the deperturbed central frequency f_0.

frequency. The absolute central frequency has been determined with a relative statistic uncertainty less than 10^{-12}, which is the main objective required to the next study on H_2^+ molecule. The residuals obtained from experimental profiles fitted by various models have enabled to develop a theoretical model taking into account of combined effects of the modulation depth, the intensity modulation induced by the frequency modulation and the hyperfine structure on the observed line shapes. This study allowed us to fix bias concerning the determination of optimal parameters involved in the two-width model and then estimate a limit width due to the transit time compatible with its expected value. This model reproduces very well the observed widths and experimental line shapes. The hypothetical origin of distinct widths due to the hyperfine structure may be tested by carrying out a similar study on a molecule which does not have a hyperfine structure. If the line shape distortions are explainable by contributions of different widths, then the hypothesis would be rejected.

6 Appendix: theoretical profile

In this appendix, we first discuss the expected line shape for an isolated transition. To that end, we summarize Arndt derivation of modulation distorted phase sensitive detection signals and extend Schilt derivation of combined intensity modulation (IM) - frequency modulation (FM) to the case of $2f_m$ IM where f_m is the frequency of the modulation frequency. We then discuss the complete line shape model and the simplified models we use.

6.1 Arndt calculation

A Lorentzian line profile centered at ν_c is given by

$$t_0(x) = \frac{1}{1+x^2} \tag{8}$$

with $x = (\nu - \nu_c)/\Delta\nu_{line}$ the reduced laser frequency. When a FM is applied, the instantaneous reduced frequency is

$$x(t) = x_0 + m\cos(2\pi f_m t) \tag{9}$$

and the time dependant spectroscopic signal is the periodic function of time

$$s(t) = t_0(x(t)) = t_0(x_0 + m\cos(2\pi f_m t), \tag{10}$$

that can be expanded in Fourier series as

$$s(t) = \sum_{n=0}^{\infty} S_n(x_0, m)\cos(2\pi\ n f_m t). \tag{11}$$

Phase sensitive detection signals are given by the Fourier coefficients $S_n(x_0, m)$ of $s(t)$. Arndt [8] has shown that

$$S_n(x_0, m) = \frac{i^n \epsilon_n}{2\ m^n} \frac{(\sqrt{(1-ix_0)^2+m^2} - (1-ix_0))^n}{\sqrt{(1-ix_0)^2+m^2}} + c.c., \tag{12}$$

with $\epsilon_0 = 1$ and $\epsilon_{n>0} = 2$.

6.2 Fabry-Perot induced IM-FM

For diode laser or quantum cascade laser sources, FM may be obtained using a modulation of the injection current. This method results in combined and phase shifted IM-FM at the same frequency. The effect of IM-FM on line shape has been studied by Schilt in [9].

In this work, we use a CO_2 laser operated very close to the maximum of the emission line. The FM at f_m is applied through the piezo-driven laser cavity length. The spectroscopy signal comes from the transmission of the Fabry Perot cavity, which is locked on resonance with the laser frequency. We have checked that this scheme results in a transmitted (and hence intracavity) IM at frequency $2f_m$ due to the quadratic behaviour of the Fabry-Perot transmission around resonance. No IM at f_m was found. We extend Schilt calculation to this case.

The instantaneous frequency and laser intensity are written

$$\begin{aligned} \nu(t) &= \nu_0 + \delta\nu_m \cos(2\pi f_m t) && (13)\\ I(t) &= I_0\left(1 + qm^2 cos^2(2\pi f_m t - \Psi)\right). && (14) \end{aligned}$$

The IM parameter

$$q = -4(\Delta\nu/\delta\nu_{FP})^2 \qquad (15)$$

is calculated in section 6.3. It depends on the Fabry-Perot HWHM $\delta\nu_{FP}$. Ψ represents a possible phase shift between IM and FM. Note that Ψ has been introduced in the intensity expression leading to much simpler calculation than in [9].

The spectroscopic signal transmitted by the cavity now reads

$$s(t) = I_0\left(1 + qm^2\cos^2(2\pi f_m t - \Psi)\right)\ t_0(x_0 + m\cos(2\pi f_m t)). \qquad (16)$$

The Fourier components of $s(t)$ can be expressed with those of $t_0(x_0 + m\cos(2\pi f_m t))$. Writing

$$s(t) = \sum_{n=0}^{\infty} S_{np}\cos(2\pi n\ f_m t) + S_{nq}\sin(2\pi n\ f_m t), \qquad (17)$$

we obtain, for $n \geq 3$

$$\begin{aligned} S_{np} &= \left(1 + \frac{qm^2}{2}\right) S_n(x,m) && (18)\\ &\quad + \frac{qm^2}{4}\cos(2\Psi)(S_{n-2}(x_0,m) + S_{n+2}(x_0,m)),\\ S_{nq} &= \frac{qm^2}{4}\sin(2\Psi)(S_{n-2}(x_0,m) - S_{n+2}(x_0,m)). && (19) \end{aligned}$$

Due to side effects, the formulas for $n = 0$, $n = 1$ and $n = 2$ are different and given by

$$\begin{aligned} S_{0p} &= \left(1 + \frac{qm^2}{2}\right) S_0(x_0,m) + \frac{qm^2}{4} S_2(x_0,m)\cos(2\Psi), && (20)\\ S_{0q} &= 0, && (21)\\ S_{1p} &= \left(1 + \frac{qm^2}{2}\right) S_1(x_0,m) && (22)\\ &\quad + \frac{qm^2}{4}\cos(2\Psi)(S_1(x_0,m) + S_3(x_0,m)),\\ S_{1q} &= \frac{qm^2}{4}\sin(2\Psi)(S_1(x_0,m) - S_3(x_0,m)), && (23)\\ S_{2p} &= \left(1 + \frac{qm^2}{2}\right) S_2(x_0,m) && (24)\\ &\quad + \frac{qm^2}{4}\cos(2\Psi)(2S_0(x_0,m) + S_4(x_0,m)),\\ S_{2q} &= \frac{qm^2}{4}\sin(2\Psi)(2S_0(x_0,m) - S_4(x_0,m)). && (25)\\ & && (26) \end{aligned}$$

Phase sensitive detection with a phase ϕ leads to the theoretical profile

$$S_{n,th}(x,m) = S_{np}(x,m)\cos(\phi) + S_{nq}(x,m)\sin(\phi). \qquad (27)$$

In the case of third harmonic detection, the theoretical line shape is

$$S_{3,th}(x,m) = A_1 S_1(x,m) + A_3 S_3(x,m) + A_5 S_5(x,m), \tag{28}$$

where

$$\begin{cases} A_1 = \dfrac{qm^2}{4}\cos(\phi - 2\Psi) \\ A_3 = \left(1 + \dfrac{qm^2}{2}\right)\cos(\phi) \\ A_5 = \dfrac{qm^2}{4}\cos(\phi + 2\Psi). \end{cases} \tag{29}$$

The coefficients A_1, A_3 and A_5 depend on q, ϕ and Ψ, which are known experimentally. In this work, the highest modulation frequency f_m=310 Hz is much smaller than the cavity HWHM (600 kHz) so the IM is in phase with the FM such that $\Psi = 0$. ϕ is chosen in order to maximize the detected signal amplitude, and corresponds to $\phi = \pi$ in our case. This leads to the lineshape fit function

$$S_{fit_1}(x,m) = A_0 - A\left(\frac{qm^2}{4}S_1(x,m) + (1 + \frac{qm^2}{2})S_3(x,m) + \frac{qm^2}{4}S_5(x,m)\right) \tag{30}$$

where A_0 is introduced to account for a signal offset and where A is positive.

6.3 Cavity width and intensity modulation

6.3.1 Pressure dependent cavity width

We consider a Fabry Perot cavity made of two identical ideal mirrors of reflectivity R and transmission $T = 1 - R$. Absorption by HCOOH in the cavity is described by the single pass amplitude transmission factor

$$\tau = e^{-\xi P/2} \tag{31}$$

where P is the pressure. The cavity finesse and maximum transmission are given by

$$F = \pi\sqrt{R\tau}/(1 - R\tau)^2 \tag{32}$$

and

$$T_{max} = (1 - R)^2\tau/(1 - R\tau)^2. \tag{33}$$

They are linked by $F^2 = F_0^2 T_{max}$. The empty cavity finesse F_0 is 153, corresponding to $R = 0.9797$ and the empty cavity HWHM is 468 kHz. We have measured the maximum transmission for $P = 0.5$, 1, 1.5 and 2 μb and fitted the results with the above formula, leading to $\xi = 5.92(17) \times 10^{-3}$ μb^{-1}. The single pass transmission τ^2 varies from 99.7 to 98.8%, the maximum transmission from 87.0 to 60.2% and the finesse from 143 to 119. The cavity HWHM given by

$$\Delta\nu_{FP} = \frac{c}{4FL}, \tag{34}$$

varies approximately linearly from 501 to 603 kHz and can be written

$$\Delta\nu_{FP} = \Delta\nu_{FP}^0 + \eta P \tag{35}$$

with $\Delta\nu_{FP}^0 = 468$ kHz and $\eta = 67.5$ kHz/μb. Eq. (35) is used in the fitting process to take into account the pressure dependant cavity width for each scan.

6.3.2 Cavity induced intensity modulation

When the cavity is locked on resonance with the laser frequency, the frequency modulation of the laser is turned into intracavity intensity modulation. Both the FM amplitude (at most 60 kHz) and the FM frequency ($f_m = 310$ Hz) are much smaller than the cavity width $\Delta\nu_{FP}$. The IM is thus determined by the quadratic behaviour of the intensity build-up close to resonance. Writing the FM $\nu(t) = \nu_0 + \delta\nu_m\cos(2\pi f_m t)$, the intracavity intensity is given by

$$I(t) = I_{max}\left(1 - 4\frac{\delta\nu_m^2}{\Delta\nu_{FP}^2}\cos^2(2\pi f_m t)\right) \tag{36}$$

where I_{max} is the maximum intensity. Using the frequency modulation parameter $m = \delta\nu_m/\Delta\nu$, we write $I(t) = I_{max}\left(1 + qm^2\cos^2(2\pi f_m t)\right)$ where the IM parameter q is given by

$$q = -4\left(\frac{\Delta\nu}{\Delta\nu_{FP}}\right)^2. \tag{37}$$

H	M_{aai}	M_{bbi}	M_{cci}
1	-6.904	0.7755	-1.305
2	-6.9275	1.0385	-0.8105

Table 7: M_{ggi} coefficients taken from [13]. Hydrogen 1 is bounded to the oxygen hydrogen 2 is bounded to the carbon atom.

7 HCOOH Hyperfine Structure

To the best of our knowledge, HCOOH hyperfine structure has only be investigated for a limited number of rotational levels in the vibrational ground state of the molecule, first by Chardon [12] and reconsidered by Cazzoli [13]. The spin of the proton attached to the oxygen (resp. carbon) atom are denoted I_1 (resp. I_2). The coupling scheme is $\mathbf{J}+\mathbf{I_1}=\mathbf{F_1}$ and $\mathbf{F_1}+\mathbf{I_2}=\mathbf{F}$. Hyperfine structure splits each HCOOH rotational level into four sublevels given by

$$E_1 = \frac{M_1+M_2}{2(J+1)} + \frac{\delta}{2(J+1)(2J+3)} \quad (38)$$

$$E_{2,3} = -\frac{M_1+M_2+\delta}{4J(J+1)} \pm \frac{1}{4J(J+1)}\left[(M_1+M_2+\delta)^2+4J(J+1)(M_1-M_2)^2\right]^{1/2} \quad (39)$$

$$E_4 = -\frac{M_1+M_2}{2J} + \frac{\delta}{2J(2J-1)}. \quad (40)$$

In these expressions,

- E_1 correponds to $F=J+1$, E_2 and E_3 to $F=J$ and E_4 to $F=J-1$.
- $M_{1,2}=\sum_{g=a,b,c} M_{gg1,2}\left\langle J_g^2\right\rangle$ where $M_{gg1,2}$ are the spin rotation constants, the label 1 (resp. 2) corresponding to the hydrogen bounded to the oxygen (resp. carbon) atom. We take the average between the experimental and theoretical values given in [13] (see Table 7). $\left\langle J_g^2\right\rangle$ are the averaged values of J_g^2 along the principal inertia axis. They are given in [12] for J=2 to 14 and small values of K_a and K_c. One can remark that $\left\langle J_a^2\right\rangle \approx K_a^2$ and that $\left\langle J_b^2\right\rangle$ is quadratic in K_c following the law $\left\langle J_b^2\right\rangle = 0.78(5)K_c^2+3.55(43)K_c+1.12(75)$. Finally, $\left\langle J_c^2\right\rangle$ is given by $J(J+1)-\left\langle J_a^2\right\rangle-\left\langle J_b^2\right\rangle$. Extrapolated values of $\left\langle J_g^2\right\rangle$ and $M_{1,2}$ to the quantum numbers relevant to this work are given in Table 8.
- δ is the spin-spin interaction matrix element. It depends on J. δ values given in [12] for J from 2 to 14 can be extrapolated with a quadratic law of the form $1.84(7)J^2-43(6)$. The extrapolation gives δ = -769(27) kHz for J=21.

The resulting hyperfine splittings are given in Table 9. Figure 8 shows the stick spectrum evaluated in the case of simple absorption spectroscopy using standard angular algebra formula (last equation in [12]). It shows that the main hyperfine components obtained for $\Delta F=0$ and $\Delta F_1=0$ form a narrow quadruplet with peaks located at $\Delta E_1=-4.4$ kHz, $\Delta E_2=0.2$ kHz, $\Delta E_3=0.0$ kHz and $\Delta E_4=4.6$ kHz from the hyperfine-less transition frequency, with respective weights 1.044, 0.998, 0.998 and 0.951. The position of the peaks mainly depends on M_1 and M_2 values with 0.2 to 0.3 kHz contributions to the uncertainties but only hardly depends on δ with less than 0.02 kHz contributions. The quadratic sum of all contributions gives an inaccuracy of about 0.5 kHz on the line position.

These four main hyperfine components span less than 10 kHz (see Fig. 8). This is slightly smaller than the transit time HWHM of the spectrometer. Hyperfine structure is unresolved but may explain the non-zero residuals of S_{fit} we observe.

Angular factors in intensities of hyperfine components in saturation spectroscopy have been evaluated by Bordé [15]. For $F \leftarrow F$ transitions in linear polarisation, they are proportional to

$$\frac{6F(F+1)-2}{30F(F+1)(2F+1)} \approx \frac{1}{10F}$$

for large values of F. The four main lines for F=20 to 22 thus have close intensities.

8 HCOOH dimerization

HCOOH dimerization equilibrium is caracterized by a dimensionless equilibrium constant [6]

$$K_{eq} = \frac{[\mathrm{HCOOH_2}]C_\phi}{[\mathrm{HCOOH}]^2} \quad (41)$$

J	K_a	K_c	$\langle J_a^2 \rangle$	$\langle J_b^2 \rangle$	$\langle J_c^2 \rangle$	M_1	M_2
21	2	20	4	387(11)	71(11)	180(9)	317(11)
21	3	19	9	353(10)	100(10)	81(9)	223(11)

Table 8: Extrapolated averaged values of the square of angular momentum components and extrapolated M_1 and M_2 coefficients.

J	K_a	K_c	E_1	E_2	E_3	E_4
21	2	20	10.9	3.3	-3.0	-12.3
21	3	19	6.5	3.6	-3.1	-7.7

Table 9: Extrapolated hyperfine structure splittings in kHz.

with $C_\phi = P_0/(RT_0)$=41.6 mol/m^3 under standard pression and temperature conditions P_0=1 atm and T_0=293.15 K. The equilibrium constant temperature dependance is

$$K_{eq} = K_0 e^{\frac{E}{k_B}(\frac{1}{T}-\frac{1}{T_0})} \tag{42}$$

with K_0=628.7 and $\frac{E}{k_B}$=7677 K. With x and $1-x$ the formic acid and dimer molar fractions, the concentrations read [HCOOH]=$x\frac{P}{RT}$ and [HCOOH$_2$]=$(1-x)\frac{P}{RT}$ and Eq. (41) leads to the second order equation

$$K_{eq}\frac{P}{P_0}\frac{T_0}{T}x^2 + x - 1 = 0, \tag{43}$$

which can be solved for x. We obtain a very small dimer molar fraction $1-x$ of 1.24×10^{-3} at room temperature (T=293.15 K) and for P=2 μb, the highest pressure used in this work.

Acknowledgements

This work was supported by LABEX Cluster of Excellence FIRST-TF (ANR-10-LABX-48-01), within the Program « Investissements d'Avenir » operated by the French National Research Agency (ANR); ANR-19-CE30-0029 HYMPE; ANR-24-CE30-00 ULTIµos; Region Ile de France DIM QUANTIP; DIM SIRTEQ (Coqteil); CPER Comb IDF; Europe EURAMET COMOMET.

References

[1] F. Guillou-Camargo, V. Ménoret, E. Cantin, O. Lopez, N. Quintin, E. Camisard, V. Salmon, J.-M. Le Merdy, G. Santarelli, A. Amy-Klein, P.-E. Pottie, B. Desruelle, and C. Chardonnet. First industrial-grade coherent fiber link for optical frequency standard dissemination. *Applied Optics*, 57(25):7203, aug 2018.

[2] Bérengère Argence, Bruno Chanteau, Olivier Lopez, Daniele Nicolodi, Michel Abgrall, Christian Chardonnet, Christophe Daussy, Benoît Darquié, Yann Le Coq, and Anne Amy-Klein. Quantum cascade laser frequency stabilization at the sub-hz level. *Nature Photonics*, 9(7):456–460, jun 2015.

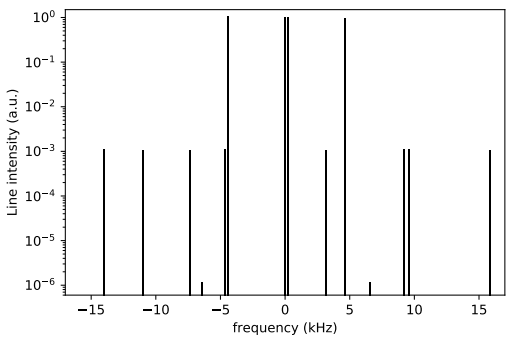

Figure 8: Stick spectrum of the fourteen hyperfine transitions in units of the reduced transition matrix element. Cross over lines are not shown.

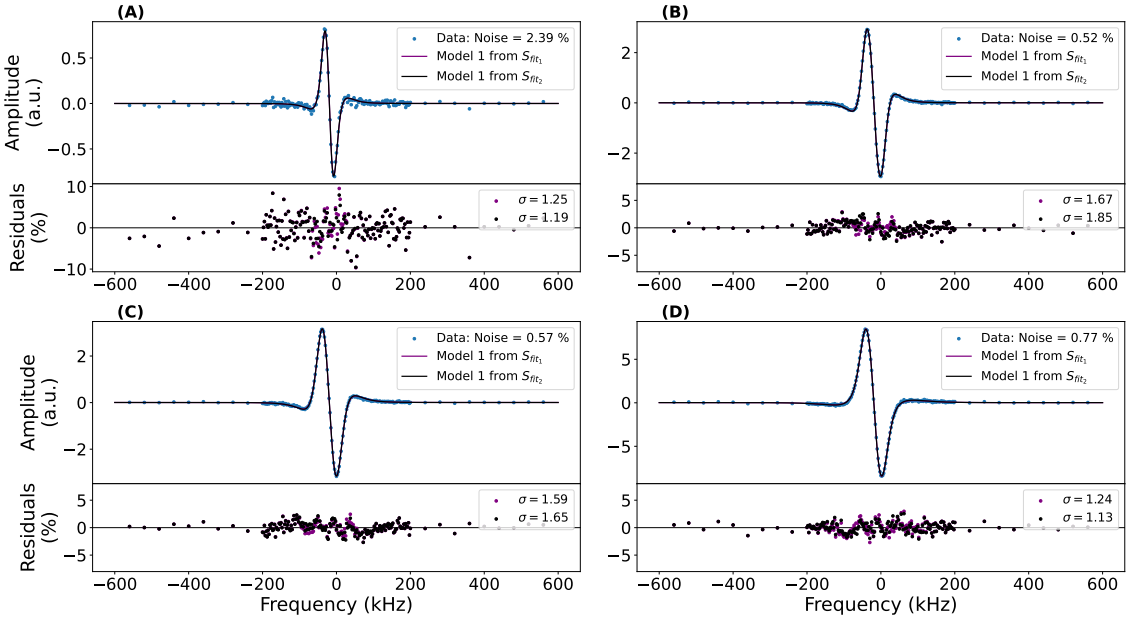

Figure 9: Experimental spectra same as in Fig. 4 compared to the corresponding simulated spectra, generated by the model n°1 with optimal parameters estimated from S_{fit_1} (purple) and S_{fit_2} (black). The experimental triplets of pressure, power and modulation depth determine the values of m_1 and m_2 in Eq. (6). The offset central frequency, global amplitude and vertical offset are adjusted. The simulated spectra are in very good agreement with experimental spectra on the entire range of values of experimental parameters.

[3] R. Santagata, D. B. A. Tran, B. Argence, O. Lopez, S. K. Tokunaga, F. Wiotte, H. Mouhamad, A. Goncharov, M. Abgrall, Y. Le Coq, H. Alvarez-Martinez, R. Le Targat, W. K. Lee, D. Xu, P.-E. Pottie, B. Darquié, and A. Amy-Klein. High-precision methanol spectroscopy with a widely tunable si-traceable frequency-comb-based mid-infrared qcl. *Optica*, 6(4):411, April 2019.

[4] Franck Bielsa, Albane Douillet, Tristan Valenzuela, Jean-Philippe Karr, and Laurent Hilico. Narrow-line phase-locked quantum cascade laser in the 9.2 μm range. *Opt. Lett.*, 32(12):1641–1643, Jun 2007.

[5] Andrew A. Mills, Davide Gatti, Jie Jiang, Christian Mohr, Will Mefford, Livio Gianfrani, Martin Fermann, Ingmar Hartl, and Marco Marangoni. Coherent phase lock of a 9 m quantum cascade laser to a 2 m thulium optical frequency comb. *Optics Letters*, 37(19):4083, September 2012.

[6] Jing Chao and Bruno J. Zwolinski. Ideal gas thermodynamic properties of methanoic and ethanoic acids. *Journal of Physical and Chemical Reference Data*, 7(1):363–377, January 1978.

[7] C. J. Bordé, J. L. Hall, C. V. Kunasz, and D. G. Hummer. Saturated absorption line shape: Calculation of the transit-time broadening by a perturbation approach. *Physical Review A*, 14(1):236–263, jul 1976.

[8] Rolf Arndt. Analytical line shapes for lorentzian signals broadened by modulation. *Journal of Applied Physics*, 36(8):2522–2524, aug 1965.

[9] Stéphane Schilt, Luc Thévenaz, and Philippe Robert. Wavelength modulation spectroscopy: Combined frequency and intensity laser modulation. *Applied Optics*, 42(33):6728, 2003.

[10] Franck Bielsa, Khelifa Djerroud, Andrei Goncharov, Albane Douillet, Tristan Valenzuela, Christophe Daussy, Laurent Hilico, and Anne Amy-Klein. Hcooh high-resolution spectroscopy in the 9.18 μm region. *Journal of Molecular Spectroscopy*, 247(1):41 – 46, 2008.

[11] Laurent Hilico, Franck Bielsa, and Anne Amy Klein. Erratum to hcooh high-resolution spectroscopy in the 9.18 μm range. *Journal of Molecular Spectroscopy*, 393:111773, mar 2023.

[12] Jean-Claude Chardon, Claude Genty, Daniel Guichon, and Jean-Gérard Theobald. rf spectrum and hyperfine structure of formic acid. *The Journal of Chemical Physics*, 64(4):1437–1441, feb 1976.

[13] G. Cazzoli, C. Puzzarini, S. Stopkowicz, and J. Gauss. Hyperfine structure in the rotational spectra of trans-formic acid: Lamb-dip measurements and quantum-chemical calculations. *Astronomy and Astrophysics*, 520:A64, sep 2010.

[14] I.E. Gordon, L.S. Rothman, R.J. Hargreaves, R. Hashemi, E.V. Karlovets, F.M. Skinner, E.K. Conway, C. Hill, R.V. Kochanov, Y. Tan, P. Wcisło, A.A. Finenko, K. Nelson, P.F. Bernath, M. Birk, V. Boudon, A. Campargue, K.V. Chance, A. Coustenis, B.J. Drouin, J.–M. Flaud, R.R. Gamache, J.T. Hodges, D. Jacquemart, E.J. Mlawer, A.V. Nikitin, V.I. Perevalov, M. Rotger, J. Tennyson, G.C. Toon, H. Tran, V.G. Tyuterev, E.M. Adkins, A. Baker, A. Barbe, E. Canè, A.G. Császár, A. Dudaryonok, O. Egorov, A.J. Fleisher, H. Fleurbaey, A. Foltynowicz, T. Furtenbacher, J.J. Harrison, J.–M. Hartmann, V.–M. Horneman, X. Huang, T. Karman, J. Karns, S. Kassi, I. Kleiner, V. Kofman, F. Kwabia–Tchana, N.N. Lavrentieva, T.J. Lee, D.A. Long, A.A. Lukashevskaya, O.M. Lyulin, V.Yu. Makhnev, W. Matt, S.T. Massie, M. Melosso, S.N. Mikhailenko, D. Mondelain, H.S.P. MÃ¼ller, O.V. Naumenko, A. Perrin, O.L. Polyansky, E. Raddaoui, P.L. Raston, Z.D. Reed, M. Rey, C. Richard, R. Tóbiás, I. Sadiek, D.W. Schwenke, E. Starikova, K. Sung, F. Tamassia, S.A. Tashkun, J. Vander Auwera, I.A. Vasilenko, A.A. Vigasin, G.L. Villanueva, B. Vispoel, G. Wagner, A. Yachmenev, and S.N. Yurchenko. The HITRAN2020 molecular spectroscopic database. *Journal of Quantitative Spectroscopy and Radiative Transfer*, 277:107949, jan 2022.

[15] J. Bordé and Ch.J. Bordé. Intensities of hyperfine components in saturation spectroscopy. *Journal of Molecular Spectroscopy*, 78(3):353–378, 1979.

9 Notations

symbol	meaning
f_{rep}	frequency comb repetition rate
ν_{CO_2}	CO_2 laser frequency
f_{beat}	beat note frequency
ν	laser frequency
ν_c	individual central frequency
$\Delta\nu_{tr}^{th}$	theoretical transit width
$\Delta\nu$	individual line width
x	normalized centered frequency
m	normalized modulation depth
$\delta\nu_m$	laser frequency modulation depth
$\Delta\nu_{FP}$	Fabry-Perot linewidth
S_n	Arndt functions
S_{fit}	S1 + S3 fit function
A_0	vertical offset
A,$A_{1,3}$	weights
D, E, F	fit coefficients
P	HCOOH Pressure
I	Laser intensity
α	pressure broadening coeff
β	coeff for the pressure dependance of the saturation intensity
I_S	saturation intensity